Bone Reports 15 (2021) 101133

Contents lists available at ScienceDirect

Bone Reports

journal homepage: www.elsevier.com/locate/bonr

Bone marrow CD73$^+$ mesenchymal stem cells display increased stemness *in vitro* and promote fracture healing *in vivo*

Kenichi Kimura [a,b,c,*], Martin Breitbach [a], Frank A. Schildberg [d], Michael Hesse [a], Bernd K. Fleischmann [a]

[a] Institute of Physiology I, Life & Brain Center, Medical Faculty, University of Bonn, D-53105 Bonn, Germany
[b] Department of Cardiac Surgery, University Hospital Bonn, D-53127 Bonn, Germany
[c] Life Science Center for Survival Dynamics, Tsukuba Advanced Research Alliance (TARA), University of Tsukuba, Ibaraki 305-8577, Japan
[d] Clinic for Orthopedics and Trauma Surgery, University Hospital Bonn, D-53127 Bonn, Germany

ARTICLE INFO

Keywords:
Mesenchymal stem cells
In vitro differentiation potential
Fracture healing
Endothelial cells

ABSTRACT

Mesenchymal stem cells (MSCs) are multipotent and considered to be of great potential for regenerative medicine. We could show recently (Breitbach, Kimura et al. 2018) that a subpopulation of MSCs as well as sinusoidal endothelial cells (sECs) in the bone marrow (BM) of CD73-EGFP reporter mice could be labeled *in vivo*.

We took advantage of this model to explore the plasticity and osteogenic potential of CD73-EGFP$^+$ MSCs *in vitro* and their role in the regenerative response upon bone lesion *in vivo*. Herein we show that isolated CD73-EGFP$^+$ MSCs displayed more pronounced stemness and stronger *in vitro* differentiation capacity into the osteogenic lineage compared to CD73-EGFP$^-$ MSCs. In a bone fracture model, endogenous BM-resident CD73-EGFP$^+$ MSCs were found to migrate to the fracture site and differentiate into cartilage and bone cells. Our analysis also showed that CD73-EGFP$^+$ sECs contributed to the neovascularization of the fracture site. In addition, grafting of CD73-EGFP$^+$ MSCs into acute bone lesions revealed their capacity to differentiate into chondrocytes and osteocytes *in vivo* and their contribution to callus formation in the regeneration process of fracture healing. Thus, CD73$^+$ MSCs display enhanced stemness and osteogenic differentiation potential *in vitro* and *in vivo* illustrating a prominent role of the CD73$^+$ MSC subpopulation to promote fracture repair.

1. Introduction

Mesenchymal stem cells (MSCs) within the bone marrow (BM) have been identified as non-hematopoietic, colony-forming cells. They exhibit distinct features, namely self-renewal and the multipotent capacity to differentiate into osteogenic, adipogenic and chondrogenic progenies *in vitro* (Pittenger et al., 1999). Cultured MSCs are well-characterized as plastic-adherent cells that express CD73, CD90 and CD105 and lack the expression of CD34, CD45, CD14, CD11b and CD19 (Dominici et al., 2006). MSCs can be isolated from a wide variety of fetal and postnatal tissues, such as placenta, umbilical cord blood, dental pulp, and fat (Erices et al., 2000; Gronthos et al., 2000; Zuk et al., 2001; Kimura et al., 2014). The potential translational use of different types of MSCs for regenerating tissues, including fracture healing, has been extensively studied. In fact, many studies suggest that transplanted MSCs contribute directly to fracture repair *via* differentiation, as grafted MSCs were found to localize on the surface of the woven bone and to differentiate into osteoblasts (Granero-Molto et al., 2009). Beyond, these cells appear to contribute also to bone healing *via* paracrine effects, as transplanted MSCs were found to secrete a variety of proinflammatory cytokines and growth factors. These were suggested to control the inflammatory response and to establish a pro-angiogenic and osteogenic milieu in the fracture site. However, many fundamental aspects of MSC biology, including their heterogeneity in dependence on tissue and donor origin as well as their subpopulations, plasticity and *in vivo* differentiation potential upon organ lesion remain relatively poorly understood.

The ecto-5′-nucleotidase CD73 is a well-known marker for cultured MSCs in mice and humans, whereas it exhibits only moderate expression in mesodermal cells (Resta et al., 1993; Chan et al., 2018). We have recently found out that in our CD73-EGFP reporter mouse unique cell populations in the BM, namely a subgroup of MSCs as well as sinusoidal

* Corresponding author at: Life Science Center for Survival Dynamics, Tsukuba Advanced Research Alliance (TARA), University of Tsukuba, Ibaraki 305-8577, Japan.
E-mail address: kkimura@tara.tsukuba.ac.jp (K. Kimura).

https://doi.org/10.1016/j.bonr.2021.101133
Received 2 August 2021; Received in revised form 11 September 2021; Accepted 24 September 2021
Available online 29 September 2021

ECs (sECs) (Breitbach et al., 2018), were specifically labeled. Interestingly, the CD73-EGFP$^+$ MSCs revealed exclusive perivascular distribution and multilineage differentiation potential *in vitro*. At this point it still remains unclear, whether and to what degree CD73$^+$ BM-derived MSCs contribute to bone repair in response to injury. Herein, we have explored the role of these cells upon bone fracture either within the same bone tissue or upon their grafting into the lesion site. Our experiments demonstrate that CD73-EGFP$^+$ expression is a marker for enhanced stemness, as CD73$^+$ MSCs were more proliferative compared to CD73$^-$ MSCs, and displayed higher differentiation potential *in vitro*. Endogenous CD73-EGFP$^+$ BM cells contributed to cartilage and bone formation during fracture repair as well as neovascularization. Furthermore, CD73-EGFP$^+$ MSCs were found to engraft into the bone fracture site after transplantation, demonstrating their prominent *in vivo* differentiation capacity to chondrocytes and osteocytes to promote bone regeneration.

2. Methods

2.1. Mice

C57BL/6J mice were purchased from Jackson laboratory (The Jackson Laboratory). CD73-EGFP mice were previously described (Breitbach et al., 2018). All mouse experiments complied with procedures approved by the regional and local Animal Care Committees. Animals were maintained on the same 12 h light/dark cycle and monitored daily by caretakers and researchers. Male and female mice of 2- to 6 months were used for cell isolation and for the bone fracture model.

2.2. Primary cultures

Bone marrow cells were isolated from femurs and tibiae of 8–10 weeks old CD73-EGFP mice. BM cells were flushed with a 21-G needle from femurs and tibiae from one animal and suspended with PBS/2% FBS. Red blood cells were removed by incubation with NH_4Cl hemolytic buffer for 2 min. Isolated cells were cultured in MEM alpha supplemented with 15% FBS, 50 U/ml Penicillin, 50 μg/ml Streptomycin (all from Invitrogen), and 5 ng/ml basic FGF (Peprotech) in a hypoxia incubator at 2% oxygen on adherent tissue culture plates (Invitrogen). Medium was changed every 3 days. Cells were trypsinized with 0.05% trypsin-EDTA (Invitrogen) at near confluence and expanded for further analysis or stored in liquid nitrogen.

2.3. Flow cytometry and cell sorting

Trypsinized cultured cells from early passage were stained with APC-labeled antibodies against CD11b (M1/70), CD44 (IM7), CD45 (30F11), Sca-1 (E13-161.7), PECAM (MEC13.3) (1:200, all from BD Pharmingen) for 20 min at 4 °C. After washing, the expression of surface markers was measured using flow cytometry (CyFlow Space). Data were analyzed with FlowJo (Tree Star). Sorting experiments were performed using a FACSAria Cell Sorter (BD Bioscience).

2.4. In vitro differentiation of MSC populations

In vitro differentiation of sorted cells was performed as described earlier with minor modifications (Breitbach et al., 2018). Cells were seeded at 3×10^4 cells/well in a 24-well plate. To induce osteogenic differentiation, cells were cultured in induction medium (0.1 μM dexamethasone, 500 μM ascorbic acid, and 10 mM β-glycerol phosphate in MEM alpha/10% FCS). The medium was changed every 3 days for 21 days, and the osteogenic ability was examined using 2% Alizarin Red solution. For quantification of osteogenic differentiation, stained cells were dissolved with 0.2 N HCL and 5% sodium dodecyl sulfate and analyzed by spectrometry at 480 nm. Adipogenic differentiation was induced by adipogenic differentiation medium (0.25 μM dexamethasone, 450 μM isobutylmethylxanthine, 1.4 μM hydrocortisone, 200 μM indomethacine, and 1.15 μM insulin in MEM alpha/10% FCS). At 21 days after induction, cells were stained with 0.5% Oil Red O solution. Cells were dissolved with 4% IGPAL CA630 (Sigma-Aldrich) in isopropanol and quantified by spectrometry at 492 nm. For chondrogenic differentiation, cells were seeded at 2×10^5 cells/well in a U-bottom 96-well plate and differentiated for 28 days in induction medium (0.1 μM dexamethasone, 500 μM ascorbic acid, 35 mM proline and 1 mM sodium pyruvate in MEM alpha/ITS-Supplement), fixed in 4% formalin and stained with 1% Alcian Blue solution. All chemicals were obtained from Sigma-Aldrich. For all differentiations, control cells were grown in MEM alpha/15% FCS.

2.5. Cell proliferation assays

Cells were plated at a density of 1×10^4 cells per 35 mm tissue culture dish in MEM alpha medium as described above. The medium was replaced with fresh medium twice a week. The number of live cells in triplicate dishes was scored using a hemocytometer at 24 h intervals for 7 days. Dead cells were excluded using trypan-blue staining solution (Sigma-Aldrich).

2.6. Immunohistochemistry

Femoral or tibial bones were fixed in 4% formalin overnight and incubated in 20% sucrose for cryopreservation. Bones were embedded in SCEM (Section-Lab Co. Ltd.) and cryosectioned (10 μm) using a cryostat (Leica CM3050S; Leica Microsystems) according to the Kawamoto method (Kawamoto, 2003). Sections were permeabilized in PBS containing 0.1% Tween 20, and blocked in PBS with 5% donkey serum for 20 min. Then, sections were stained with rat anti-osteopontin (DSHB), rat anti-PECAM (MEC13.3), rat anti-Vcam1 (MVCAM.A) (BD Pharmingen), goat anti-c-kit, goat anti-endomucin (R&D systems), rat anti-CD45 (IBL-5/25) (Merck Millipore), rat anti-endomucin (V.7C7) (Santa Cruz Biotechnology) and rabbit anti-aggrecan (Merck Millipore). Cultured cells were fixed in 4% formalin and permeabilized with PBS containing 0.1% Tween 20. Cells were blocked in PBS with 5% donkey serum and stained with rat anti-CD73 (TY/23, BD Pharmingen). To visualize primary antibodies and nuclei, Cy3- or Cy5-conjugated secondary donkey antibodies (all from Jackson ImmunoResearch) and Hoechst 33342 (Sigma-Aldrich) were applied for 1 h at room temperature. Images were taken with an inverted fluorescence microscope (Axiovert 200) equipped with a slider module (ApoTome; Carl Zeiss MicroImaging) and a confocal microscope (ECLIPSE Ti; Nikon).

2.7. Bone repair analysis

All animal experiments were performed in accordance with the Guide for the Care and Use of Laboratory Animals published by the National Institutes of Health (8th edition, revised 2011) and were approved by the local ethics review board (Landesamt für Natur, Umwelt und Verbraucherschutz Nordrhein-Westfalen, Germany, #84-02.04.2013.A427). The bone fracture mouse model was performed, as reported earlier (Kimura et al., 2014): In brief, the mice were anesthetized, next the skin on the lateral hind limb was incised and the femur exposed *via* dissection through the fascial plane between the anterior and posterior muscle compartments. The defect was created with a fine scissor, then a 27G needle was passed into the medullary canal to fix the bone fracture. Sorted and cultured EGFP$^+$ or EGFP$^-$ MSCs from BM of CD73-EGFP mice (5×10^5 cells) were embedded in 2×2 mm absorbable gelatin sponge, Gelfoam (Pfizer) and transplanted into the defects; as control, Gelfoam with saline was used. For postoperative analgesia, buprenorphin was injected subcutaneously at 0.1 mg/kg body weight every 12 h for at least 3 days. After 7, 14 and 28 days, bone regeneration at the fracture site was examined by immunohistology, as well as von Kossa-, and HE stainings.

2.8. Real-time PCR

Cells were pelleted and homogenized in TRIzol (Invitrogen). RNA was isolated following the manufacturer's protocol and traces of DNA were removed by DNAse treatment (Qiagen). Integrity of RNA extracts was assessed on a 1% MOPS gel. First strand complementary DNA (cDNA) was synthesized using the SuperScript VILO cDNA Synthese Kit (Invitrogen). Real-time PCR was performed on a Corbett Rotor-Gene 6000 real time PCR cycler (Qiagen) using TaqMan gene expression master mix and assays for CD73 (Mm01144395_m1), EGFP (Mr04329676_mr) and 18S rRNA (Hs99999901_s1) (all from TaqMan® Gene Expression Assays, Thermo Fischer Scientific). CD73 and EGFP expression were normalized using 18S rRNA as an internal control. Results are expressed in fold change values compared with mean expression levels (ΔΔCt method).

2.9. Quantification and statistical analysis

All data are represented as mean ± SEM, a p-value of <0.05 was considered statistically significant. Images were analyzed for quantification using Image J and at least three sections, total >600 cells, were examined except in Fig. 5C from one section, total >70 cells. Quantification of cell shape, EGFP and CD73 expression was also analyzed using image J. The morphology of EGFP$^+$ and EGFP$^-$ cells was evaluated using the cell shape index, CSI, which uses the following equation: $CSI = 4\pi \times Area / (Perimeter)^2$ (Versaevel et al., 2012). Correlation of EGFP and CD73 fluorescence was assessed using a non-parametric Spearman correlation analysis. Statistical significance was assessed by two-sided Student's t-test, or one-way ANOVA with Tukey's post-hoc test, where applicable.

3. Results

3.1. Isolation and characterization of CD73-EGFP$^+$ cells from BM

Whole BM cells were isolated from femurs and tibiae of 8 to 10 weeks old transgenic CD73-EGFP mice and cultured. From day 5 in culture, BM cells gave rise to fibroblastic colonies showing EGFP expression and MSC-like morphology (Fig. 1A). Previously, we demonstrated that CD73 expression is an indicator of increased plasticity of MSCs (Breitbach et al., 2018). Therefore, in order to explore the function of CD73-EGFP$^+$ and EGFP$^-$ MSC subpopulations in more detail, we expanded primary BM cells for two passages and subsequently sorted CD73$^+$ and CD73$^-$ populations based on EGFP expression using flow cytometry (Fig. 1B). The EGFP$^+$ cells displayed preferentially a long spindle-shaped morphology and preserved EGFP fluorescence as can be seen in representative pictures (Fig. 1C, Supplementary Fig. 1A, B). This was further supported by unbiased imaging analysis, illustrating that EGFP$^+$ cells clearly have a more elongated (spindle) shape, as compared to EGFP$^-$ cells in both MSC populations (CSI; 0.53 ± 0.02 in EGFP$^-$ cells in EGFP$^-$ fraction, $n = 69$; 0.54 ± 0.04 in EGFP$^-$ cells in EGFP$^+$ fraction, $n = 30$; 0.39 ± 0.04 in EGFP$^+$ cells in EGFP$^+$ fraction, $n = 34$, $p < 0.01$, one-way ANOVA, Supplementary Fig. 1A). qPCR experiments revealed significantly stronger expression levels of EGFP and CD73 for the EGFP$^+$ population compared to the EGFP$^-$ control fraction, which was observed up to passage 6 (Fig. 1D, E). Importantly, we found a very good correlation between EGFP and CD73 protein expression using anti-CD73 immunostaining for cultured EGFP$^+$ and EGFP$^-$ MSC subpopulations (Fig. 1F) and also for BM-derived cells; this was also corroborated when measuring EGFP and CD73 fluorescence in EGFP$^+$ and EGFP$^-$ cells ($n >$ 150) yielding a significant correlation of 0.79 (data not shown).

Next, we investigated cell surface marker expression and the *in vitro* differentiation potential of EGFP$^+$ and EGFP$^-$ MSCs isolated from CD73-EGFP mice in order to define potential differences between these two populations in more detail. Flow cytometry analysis of cultured cells after two passages revealed that typical MSC markers, such as Sca-1 and CD44 (Baddoo et al., 2003), were detected on the majority of both EGFP$^+$ and EGFP$^-$ MSCs (Sca-1; 78.4% of EGFP$^+$ MSCs *vs.* 64.9% of EGFP$^-$ MSCs, CD44; 99.8% of EGFP$^+$ MSCs *vs.* 98% of EGFP$^-$ MSCs, Fig. 2A). EGFP$^+$ MSCs proved negative for the blood lineage marker CD45 and CD11b, whereas the EGFP$^-$ fraction contained a low percentage of positive cells (CD45; 1.1% of EGFP$^+$ MSCs *vs.* 10.9% of EGFP$^-$ MSCs, CD11b; 0.8% of EGFP$^+$ MSCs *vs.* 8.9% of EGFP$^-$ MSCs). Based on our earlier findings, namely that CD73-EGFP mice also labeled specific BM ECs (Breitbach et al., 2018), we analyzed also expression of the endothelial marker CD31 in both fractions of cells. Our data revealed that, as expected from the cell culture protocol, both populations were negative for this marker, excluding the presence of ECs in the *in vitro* cultures.

The *in vitro* differentiation potential of the EGFP$^+$ and EGFP$^-$ MSC populations was assessed using standard differentiation protocols for MSCs into osteogenic, adipogenic and chondrogenic lineages (Fig. 2B). Both populations could be differentiated to similar degrees into adipocytes, whereas the osteogenic and chondrogenic differentiation potential was clearly higher in the EGFP$^+$ cell fraction. To underscore this quantitatively, we dissolved stained cells and performed absorbance measurements by spectrophotometry. These experiments proved that the EGFP$^+$ MSCs showed a significantly higher osteogenic differentiation potential (osteogenic differentiation: absorbance 480 nm; 0.61 ± 0.04 in EGFP$^+$ MSCs *vs.* 0.13 ± 0.01 in EGFP$^-$ MSCs, $n = 3$, $p < 0.01$; adipogenic differentiation: absorbance 492 nm; 0.08 ± 0.002 in EGFP$^+$ MSCs *vs.* 0.07 ± 0.01 in EGFP$^-$ MSCs, n = 3, not significant, two-sided t-test, Fig. 2C, D).

Using a standard proliferation assay, we also determined numbers of viable cells at day 1, 3, 5- and 7-days post-plating. We found that the EGFP$^+$ MSC populations revealed a higher proliferation capacity compared to EGFP$^-$ MSCs at day 3, and the observed differences significantly increased over time (doubling time; 19.1 ± 1.4 h in EGFP$^+$ MSCs, 22.8 ± 1.3 h in EGFP$^-$ MSCs, n = 3, p < 0.01, two-sided t-test, Fig. 2E). Overall, the EGFP$^+$ MSCs showed typical MSC marker expression, and strongly enhanced tri-lineage differentiation and self-renewal capacity compared to EGFP$^-$ MSCs underscoring enrichment for highly potent MSCs in the EGFP$^+$ population.

3.2. Endogenous CD73$^+$ BM-MSCs contribute to fracture repair

Bone fracture is an injury affecting the structural continuity of the bone cortex. Fracture healing consists of multiple events, including hematoma, fibrocartilaginous and bony callus formation as well as bone remodeling. The generation of callus tissues is known to be critically dependent on the recruitment of MSCs from the surrounding tissue and BM (Kumar and Ponnazhagan, 2012). Therefore, fracture healing models are very well suited to explore the cellular dynamics of MSC migration and differentiation upon tissue regeneration.

Given the pronounced osteogenic differentiation potential of the EGFP$^+$ cells and our earlier findings that EGFP$^+$ cells contribute to endochondral ossification at the embryonic stage (Breitbach et al., 2018), we next explored the endogenous plasticity of the EGFP$^+$ MSC subpopulation in the adult stage *in vivo*. To this aim, we performed, as reported by our group before (Kimura et al., 2014), a surgical fracture with internal fixation of the femur in 2 months old CD73-EGFP transgenic mice (Fig. 3A, B). At day 4 after the fracture, we could observe EGFP$^+$ cells at the border of the bone apparently migrating towards the fracture site (Fig. 3C). These cells expressed the bone lining cell marker osteopontin, but neither the endothelial marker endomucin (EMCN) nor the blood lineage marker CD45 (Fig. 3D, E), suggesting that these are most likely MSC-like BM cells. At day 7 after fracture, we could observe large numbers of EGFP$^+$ cells in the area of the periosteum, and some EGFP$^+$ cells contributing to cartilage formation (Fig. 3F). In the internal callus, a substantial increase of EGFP$^+$ cells could be observed in the border zone of the cartilage formation area, roughly 60% of the chondrocytes in the internal callus were found to be EGFP$^+$ (Fig. 3G, $n = 3$

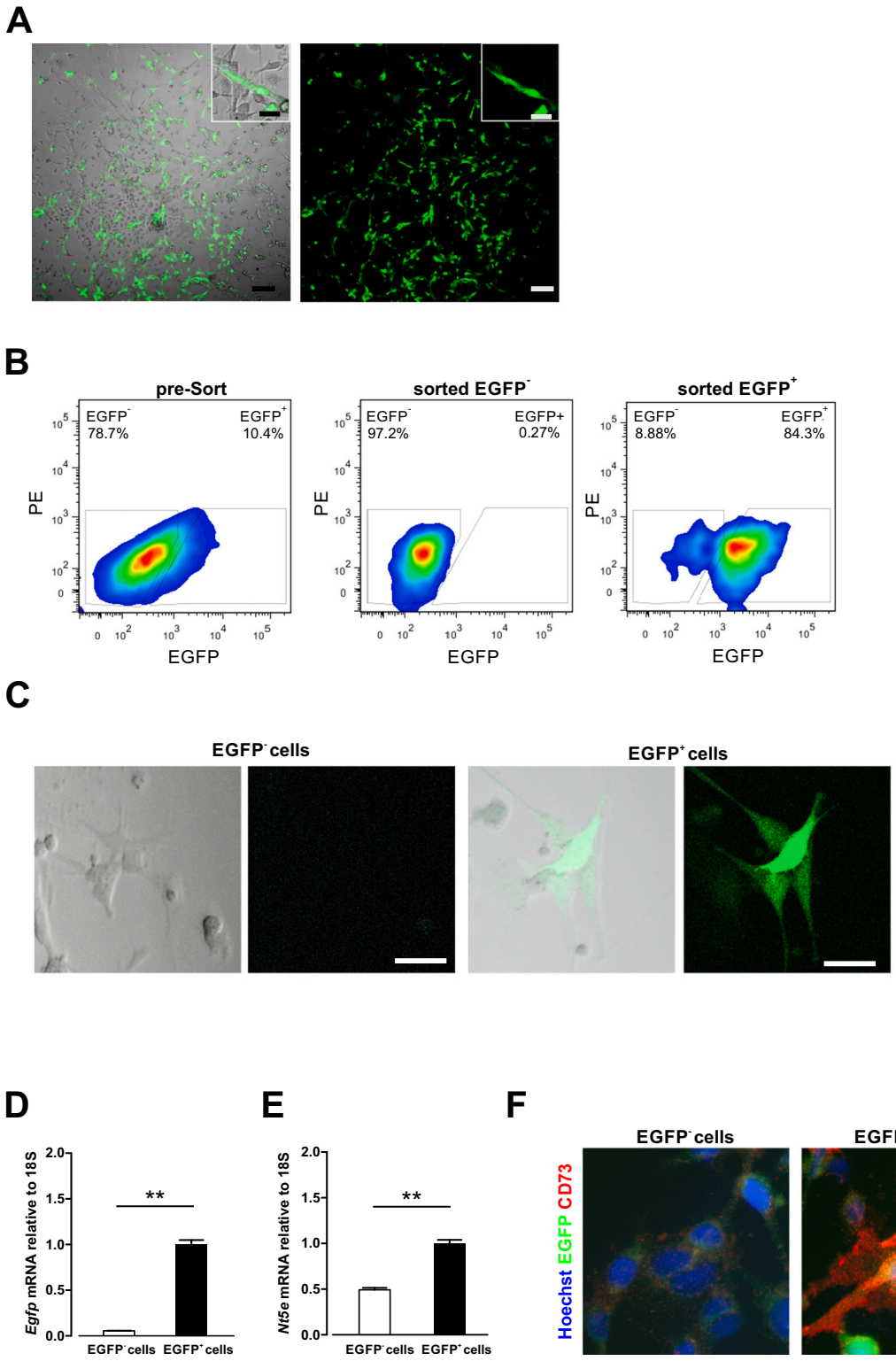

Fig. 1. Isolation and characterization of CD73-EGFP^{+} cells from BM.
(A) EGFP^{+} colonies containing EGFP^{-} cells of primary BM cultures displayed typical MSC-like morphology at day 5 in culture. Scale bars 100 μm, insets 10 μm. (B) EGFP^{+} and EGFP^{-} cell fractions were sorted by flow cytometry from passage 2 to 3 of a whole BM cell culture. (C) Sorted EGFP^{+} cells showed EGFP fluorescence at passage 5 in culture. Scale bars 10 μm. (D, E) Cultured EGFP^{+} cells preserved EGFP (D) and *Nt5e* (CD73) (E) expression at passage 6 in culture as assessed by realtime PCR. (F) Anti-CD73 staining revealed CD73 expression in EGFP^{+} cells. Scale bar 10 μm. $n = 3$, two-sided *t*-test, **: $P < 0.01$.

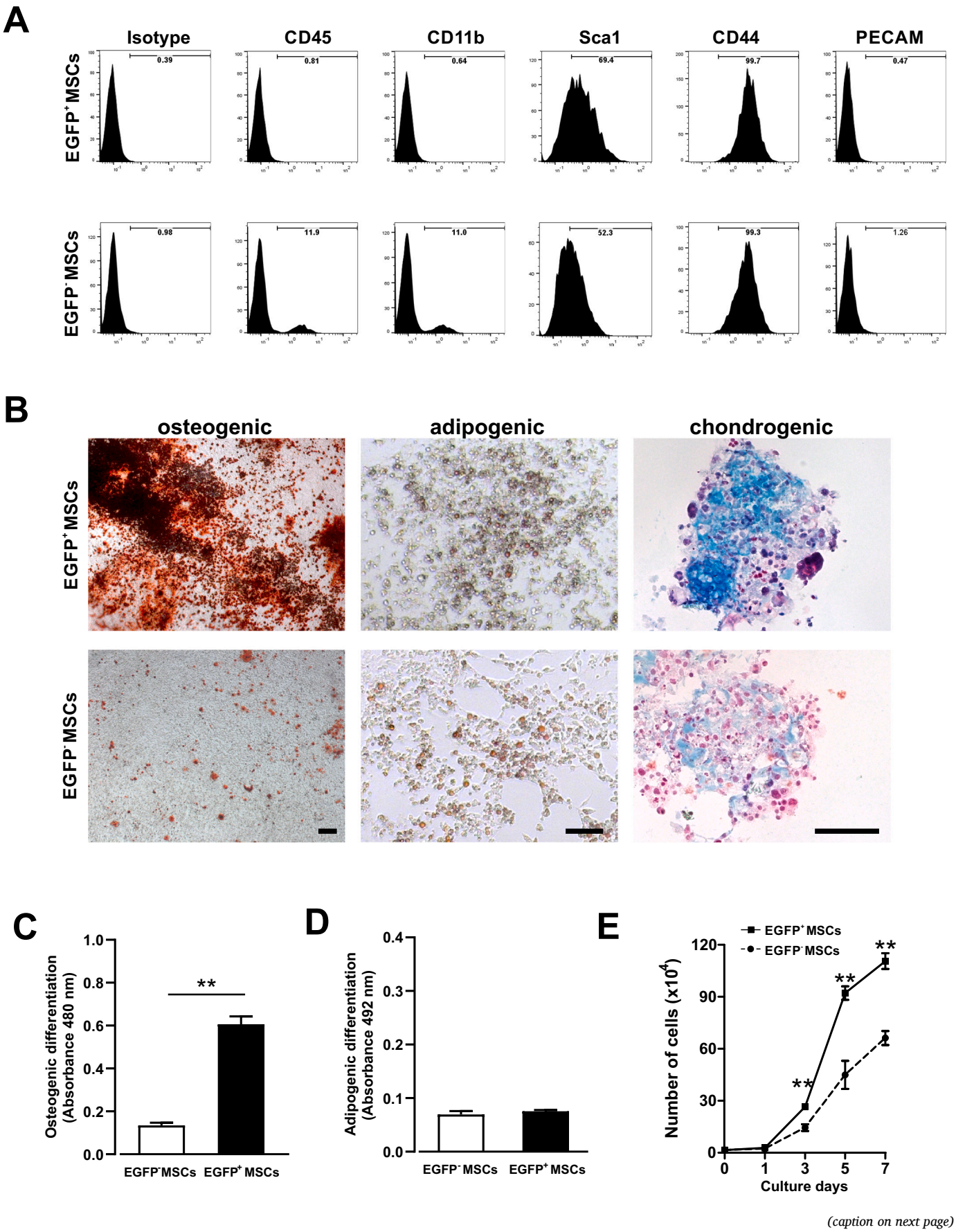

(caption on next page)

Fig. 2. Characterization of cultured CD73-EGFP$^+$ and EGFP$^-$ MSCs.
(A) Cultured BM-derived EGFP$^+$ and EGFP$^-$ MSCs from 2 to 3 passages after sorting for EGFP were found to express typical MSC markers in flow cytometry. (B) Comparison of *in vitro* differentiation potential of EGFP$^+$ and EGFP$^-$ MSCs into osteoblasts (alizarin red), adipocytes (oil red O) and chondrocytes (trypan blue) revealed strongly increased osteogenic and chondrogenic fate. Scale bars 100 μm. (C, D) After staining, absorbance measurements of cells differentiated into osteogenic (C) or adipogenic (D) fates at day 21 underscored the enhanced osteogenic potential of EGFP$^+$ MSCs. n = 3, two-sided t-test, **: P < 0.01. (E) Comparison of the cell proliferation capacity of EGFP$^+$ and EGFP$^-$ MSCs in culture yielded significantly higher values for EGFP$^+$ MSCs until reaching confluence. n = 3, two-sided t-test, **: P < 0.01.

sections). In addition, in the area of bone trabeculae within the internal callus, some osteopontin$^+$ osteoblasts were EGFP$^+$ implying that EGFP$^+$ MSCs differentiated into osteoblasts at day 7 after the lesion (Fig. 3H). Moreover, at day 14 after fracture, EGFP$^+$ cells were observed within the bone trabeculae, indicating their further differentiation into mature osteocytes (Fig. 3I, J). These data suggest that endogenous CD73-EGFP$^+$ cells directly contribute to bone regeneration by differentiating into mesenchymal derivatives *in vivo*.

In the CD73-EGFP transgenic mice we found that BM sECs were also EGFP$^+$, whereas the other BM ECs were EGFP$^-$ (Breitbach et al., 2018). Therefore, we investigated the potential contribution of these ECs to angiogenesis and reconstitution of the hematopoietic niche in the BM during fracture healing. At day 7 after fracture, Vcam1, known to be involved in hematopoietic stem cell (HSC) retention and strongly expressed in sECs, was found to be consistently expressed in EGFP$^+$ sECs in non-injured BM areas (Fig. 4A). In contrast, Vcam1 expression was lacking in neovascular ECs (Fig. 4B), and none of these cells expressed EGFP in the regenerative areas within the internal callus. This proved to be different at later stages (day 14 post-lesion) of fracture healing, as double positive Vcam1$^+$/EGFP$^+$ neovascular ECs could be observed in the regenerative area within the callus (Fig. 4C). To better understand the potential cellular crosstalk between EGFP$^+$ cells and the HSC niche, we analyzed the distribution of c-kit$^+$ HSC/progenitor cells. We could observe newly formed BM containing c-kit$^+$ cells in part of the callus (Fig. 4D). These c-kit$^+$ cells located in close vicinity to EGFP$^+$ newly formed vessels (Fig. 4E), whereas there were no c-kit$^+$ cells in the bone trabeculae within regenerating bone regions (Fig. 4F). Thus, these data suggest that EGFP$^+$ cells contribute to the neovascularization of the lesion site and might also support reconstitution of the hematopoietic niche during fracture repair.

3.3. Grafted CD73-EGFP$^+$ MSCs contribute to fracture repair by forming bone and cartilage

The endogenous CD73-EGFP$^+$ MSCs displayed *in vivo* differentiation potential into bone and cartilage cells in response to injury. Thus, to probe the plasticity and impact of CD73-EGFP$^+$ MSCs upon fracture healing, we grafted cultured BM-derived EGFP$^+$ MSCs into the fracture site and compared this to the grafting of EGFP$^-$ MSCs. We embedded 5 × 10^5 cultured BM-derived EGFP$^+$ or EGFP$^-$ MSCs into 2 mm × 2 mm gelatine sponges and transferred these into the fracture site at the time of the injury (Fig. 5A). No EGFP$^+$ cells were detected in the saline control groups (Fig. 5B), whereas EGFP$^+$ MSCs were found to differentiate into aggrecan$^+$ chondrocytes in the regenerative area at day 7 after fracture (EGFP$^+$ cells: 26.3% ± 4.2% of aggrecan+ cells, $n = 3$ sections, Fig. 5C). Furthermore, grafted EGFP$^+$ MSCs could be found within the bone trabeculae at the site of the fracture callus formation, indicating differentiation into osteocytes (EGFP$^+$ cells: 2.8% in bone trabecular cells, $n = 1$ section, Fig. 5D). In order to assess their potential impact on the bone repair process, we quantified the degree of bony callus formation using von Kossa staining (Fig. 5E). Our analysis revealed that the grafting of EGFP$^+$ MSCs significantly enhanced new bone formation in the external callus area compared to the grafting of EGFP$^-$ MSCs or saline injection (Fig. 5F). Moreover, we also analyzed the fracture gap at 28 days after the lesion and found that in the EGFP$^+$ MSC group it was filled with new bone callus, whereas this was neither the case in the EGFP$^-$ MSC nor saline injection groups (Fig. 5G). The areas formed by bony callus were significantly larger in the EGFP$^+$ MSC group, compared to either EGFP$^-$ or control groups (control group: 24.9% ± 3.8%, $n = 4$ mice; EGFP$^-$ MSC group: 27.3% ± 2.5%, $n = 6$ mice; EGFP$^+$ MSC group: 34.7% ± 3.2%, $n = 5$ mice; v.s. EGFP$^+$ MSC group, $p < 0.01$, one-way ANOVA, Fig. 5H). Furthermore, the fracture gap of the EGFP$^+$ group was mainly composed of lamellar bone, whereas that of the EGFP$^-$ MSC group contained mainly fibrous and cartilaginous tissue (Fig. 5I). Thus, these data revealed that CD73 is a suitable marker to enrich for a MSC subpopulation that gives rise to chondrocytes and osteocytes after transplantation *in vivo* promoting bone formation and hence fracture repair.

4. Discussion

Aim of this study was to investigate the plasticity of CD73$^+$ BM-MSCs *in vitro*, and their impact and role for endogenous repair in response to bone fracture and upon grafting of these cells into the lesion site *in vivo*. Our data demonstrate that this MSC subpopulation displays high stemness and cellular plasticity, as proven by their enhanced differentiation potential into osteogenic and chondrogenic lineages *in vitro* and *in vivo*. This suggests that this MSC subpopulation is particularly suited for cell-based bone repair approaches.

BM-MSCs are very rare stromal cells that have self-renewal potential and the capacity to differentiate into mesenchymal derivatives. Because of the lack of a specific cell surface marker MSCs can only be identified *via* determining the presence and absence of a multitude of different markers (Sacchetti et al., 2007; Crisan et al., 2008; Chou et al., 2012). Given that the identification and purification of BM-MSCs is complicated due to the lack of a reliable marker, these cells are preferentially isolated using adherence cell culture, resulting in rather heterogeneous MSC populations. In the present work, we have therefore taken advantage of a transgenic mouse model, which enables identification and purification of BM-MSCs based on their CD73-EGFP expression. We found that the CD73$^+$ BM-MSC subpopulation displays a greater degree of stemness compared to CD73$^-$ BM-MSCs, as underscored by shortened population doubling times. Earlier studies could provide a hint for possible mechanisms, since CD73 has been proposed as a critical factor for cell proliferation (Zhang, 2012). A striking observation in regard to the plasticity of CD73$^+$ BM-MSCs was their clearly enhanced differentiation potential into osteogenic and adipogenic lineages *in vitro*. In the present work, we have used CD73 as a marker system to identify MSCs, but at this time we do not know, whether CD73-signaling itself is involved in this enhanced stemness and/or osteogenic differentiation. CD73 is known to play an important role in the cleavage of extracellular AMP to adenosine in the ATP degradation pathway, and adenosine signaling regulates a wide variety of physiological processes. In fact, it has been reported that adenosine receptor stimulation enhances proliferation and osteogenic differentiation of MSCs and osteoblasts *in vitro* (D'Alimonte et al., 2013) (Costa et al., 2011) (Takedachi et al., 2012) (Ode et al., 2013). Furthermore, osteoblast activation through CD73 activity has been reported to be essential for bone repair in aged mice (Bradaschia-Correa et al., 2017). Earlier studies have shown that adenosine signaling *via* A2B receptor regulates osteoblast differentiation, bone formation, and fracture repair in the A2B KO mice (Carroll et al., 2012).Therefore, we are aiming to explore in the future, whether CD73 and/or adenosine receptor-dependent signaling are involved in the increased stemness and the strongly enhanced *in vitro* differentiation potential of CD73-EGFP$^+$ MSCs into the osteogenic- and adipogenic lineages using a combination of biochemical, inducible knock-down and pharmacological strategies.

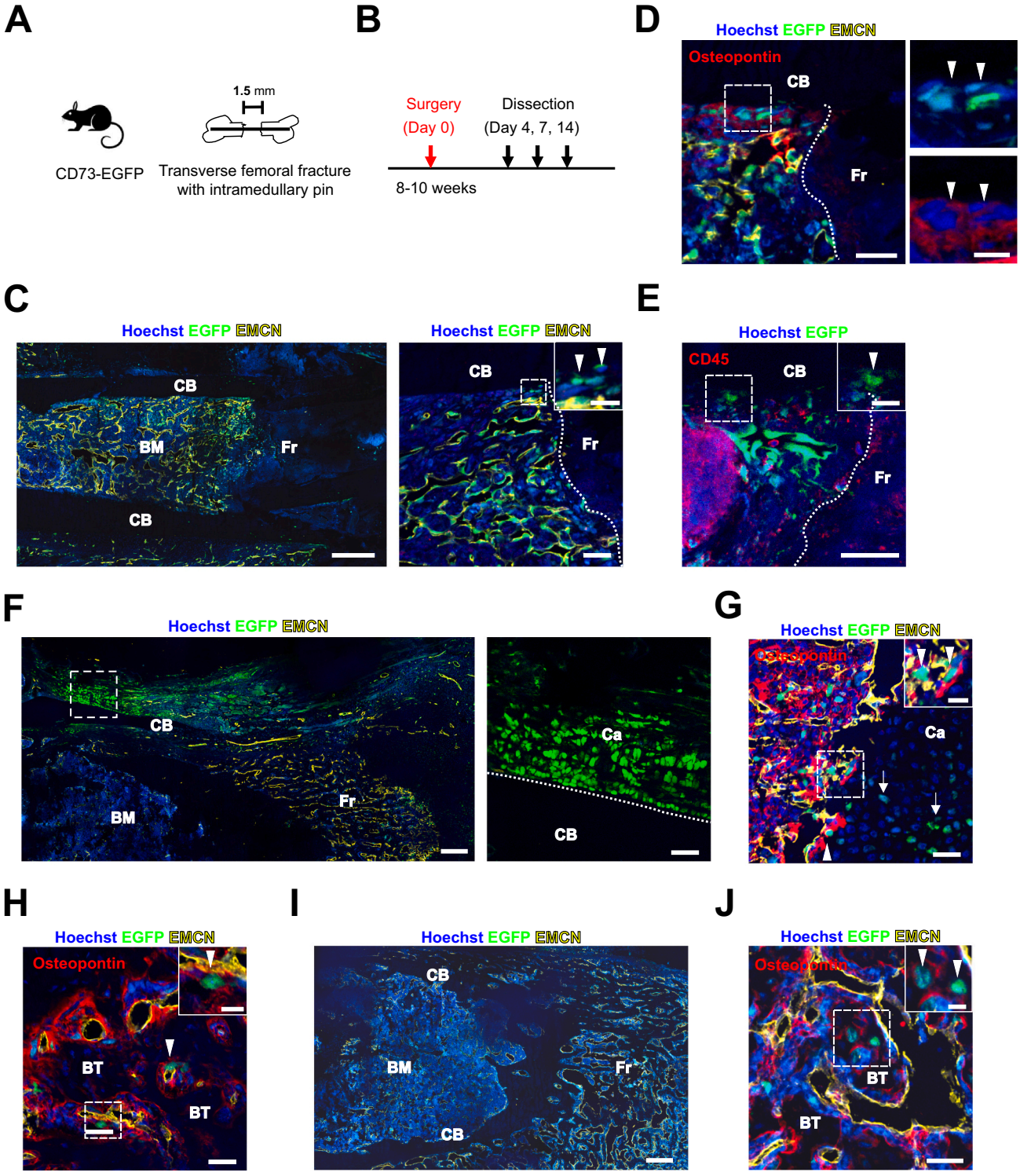

Fig. 3. CD73-EGFP^{+} BM cells differentiate into chondrocytes and osteoblasts upon fracture and fracture healing.
(A) Experimental scheme of the transverse femoral fracture model. (B) Timeline of fracture generation and analysis. (C-E) Representative confocal images of a femoral section through the fracture site. Immunofluorescence staining against endomucin (EMCN) at day 4 after fracture is shown (C, D). Arrowheads mark EGFP^{+} cells migrating towards the fracture site (C). These cells are also osteopontin^{+} (D), but CD45^{-} (E); the boxed area is shown in the magnified image to the right, and insets are taken from the boxed area, respectively. Scale bars 100 μm (C, left), 25 μm (C right, D, E), insets 10 μm (C-E). (F) Representative confocal images of femoral sections at day 7 after the lesion. Localization of EGFP^{+} cells in the periosteum and fracture callus of a CD73-EGFP^{+} mouse. In the periosteum, large numbers of EGFP^{+} cells were apparent in the cartilage; the boxed area is shown in the magnified image to the right. Scale bars 100 μm, magnified image 25 μm. (G-J) Immunofluorescence stainings against EMCN and osteopontin show that EGFP^{+} cells migrated into the border zone (arrowheads) of cartilage formation area within internal callus and differentiated into chondrocytes (arrows) (G) and osteopontin^{+} osteoblasts (arrowheads) in the area of bone trabeculae within internal callus (H). Representative image of femoral section at day 14 after the lesion (I). At day 14 after fracture, the EGFP^{+} cells are observed within bone trabeculae in the internal callus (arrowheads) (J); insets are taken from the boxed areas, respectively. Scale bars 100 μm (I), 25 μm (G, H J), insets 10 μm (G, H J). Hoechst staining of nuclei and EGFP revealing native fluorescence. CB: cortical bone. Fr: fracture site. Ca: cartilage. BT: bone trabeculae. BM: bone marrow.

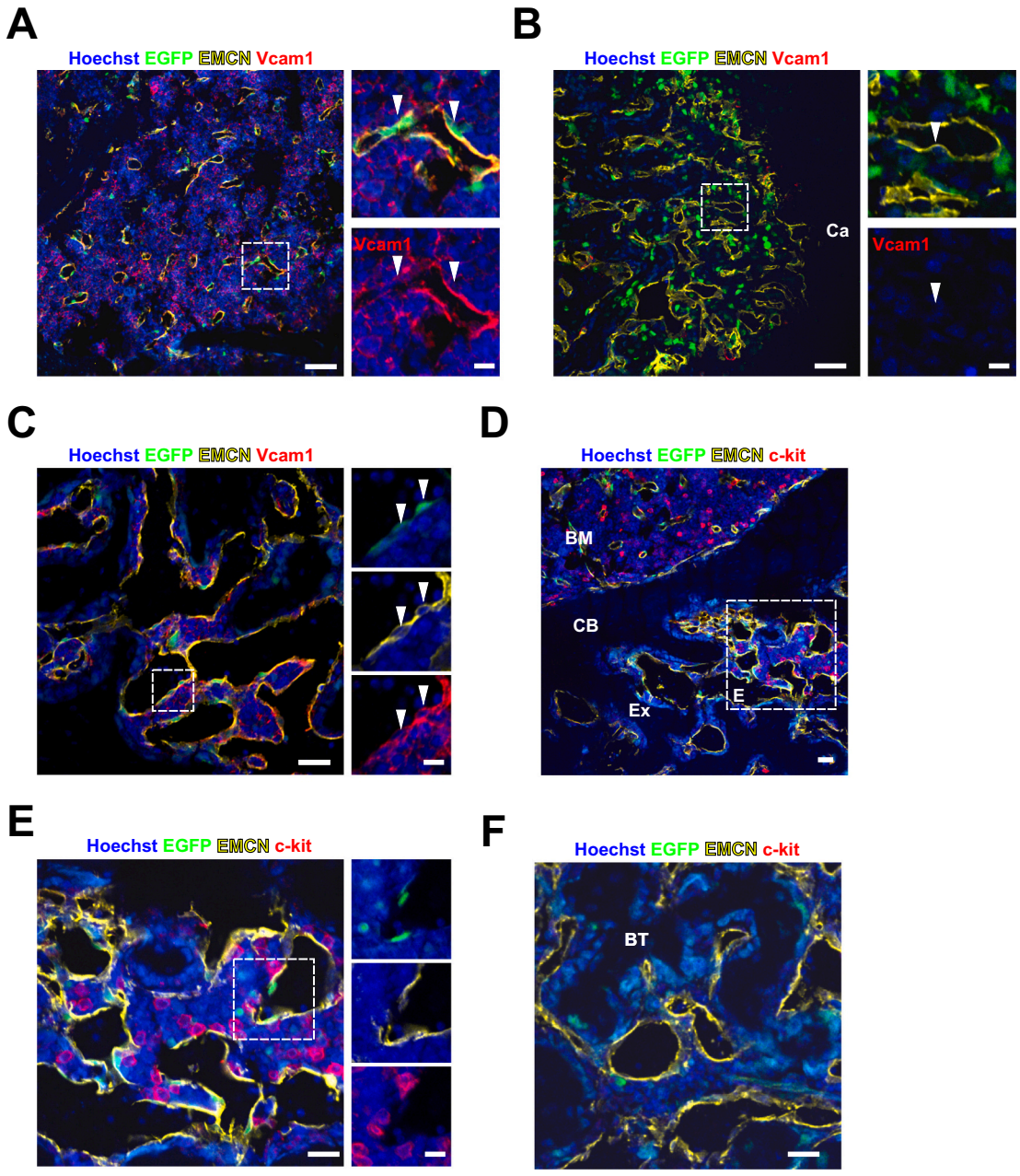

Fig. 4. CD73-EGFP$^+$ cells contribute to neovascularization in the fracture site.
(A, B) Vcam1 expression was detected on EMCN$^+$/EGFP$^+$ sinusoidal endothelial cells (sECs) in the non-injured BM area (arrowheads) (A), but not on ECs of newly formed vessels in the regenerative area within the internal callus (arrowhead) (B) at day 7 after fracture; right panels are magnified from the boxed areas, respectively. Scale bars 50 μm. (C) ECs in newly formed vessels were found to be EGFP$^+$ and Vcam1$^+$ (arrowheads) in the regenerative area at day 14 after fracture; right panels are magnified from the boxed area. Scale bar 25 μm. (D, E, F) C-kit$^+$ hematopoietic cells were found in the external callus (D); the boxed area is shown in the magnified image (E). C-kit$^+$ cells colocalize with EGFP$^+$ ECs of newly formed vessels in the external callus (E), but not in the trabecular bone areas (F), as underscored by immunostainings at day 14 after fracture; right panels are magnified from the boxed area in (E). Scale bars 25 μm, magnified images 10 μm. CB: cortical bone. Ca: cartilage. BM: bone marrow. Ex: external callus. BT: bone trabeculae.

The observation of the enhanced *in vitro* differentiation characteristics of CD73-EGFP+ MSCs motivated us to investigate this aspect also *in vivo* using a bone fracture model. MSCs are activated in the early phase of bone regeneration and well known as main contributors to bone remodeling. However, their endogenous origins and the mechanisms of activation during bone fracture repair still remain largely unresolved. Elegant fate mapping studies have revealed that *Lepr*-cre$^+$ and *Cxcl12*-creER$^+$ BM stromal cells respond to stress and contribute to bone regeneration during fracture healing (Zhou et al., 2014) (Matsushita et al., 2020), whereas perivascular cells behaved as MSCs *in vitro*, but did not contribute to other cell lineages *in vivo* (Guimaraes-Camboa et al., 2017). Herein, we have observed that resident CD73-EGFP$^+$/EMCN$^-$ BM cells migrate towards the fracture site and accumulate at the boundary of cartilage in the internal callus, and that the progeny of CD73$^+$ MSCs give rise to newly formed cartilage and bone. Thus, our data suggest that CD73$^+$ MSCs are a very interesting subpopulation, as they respond to injury and participate in the repair process. Interestingly, earlier work reported that skeletal stem cells identified as CD51$^+$CD90$^-$CD105$^-$CD200$^+$ cells in the BM can generate a variety of cells of the skeletal lineage and display strong potential to differentiate

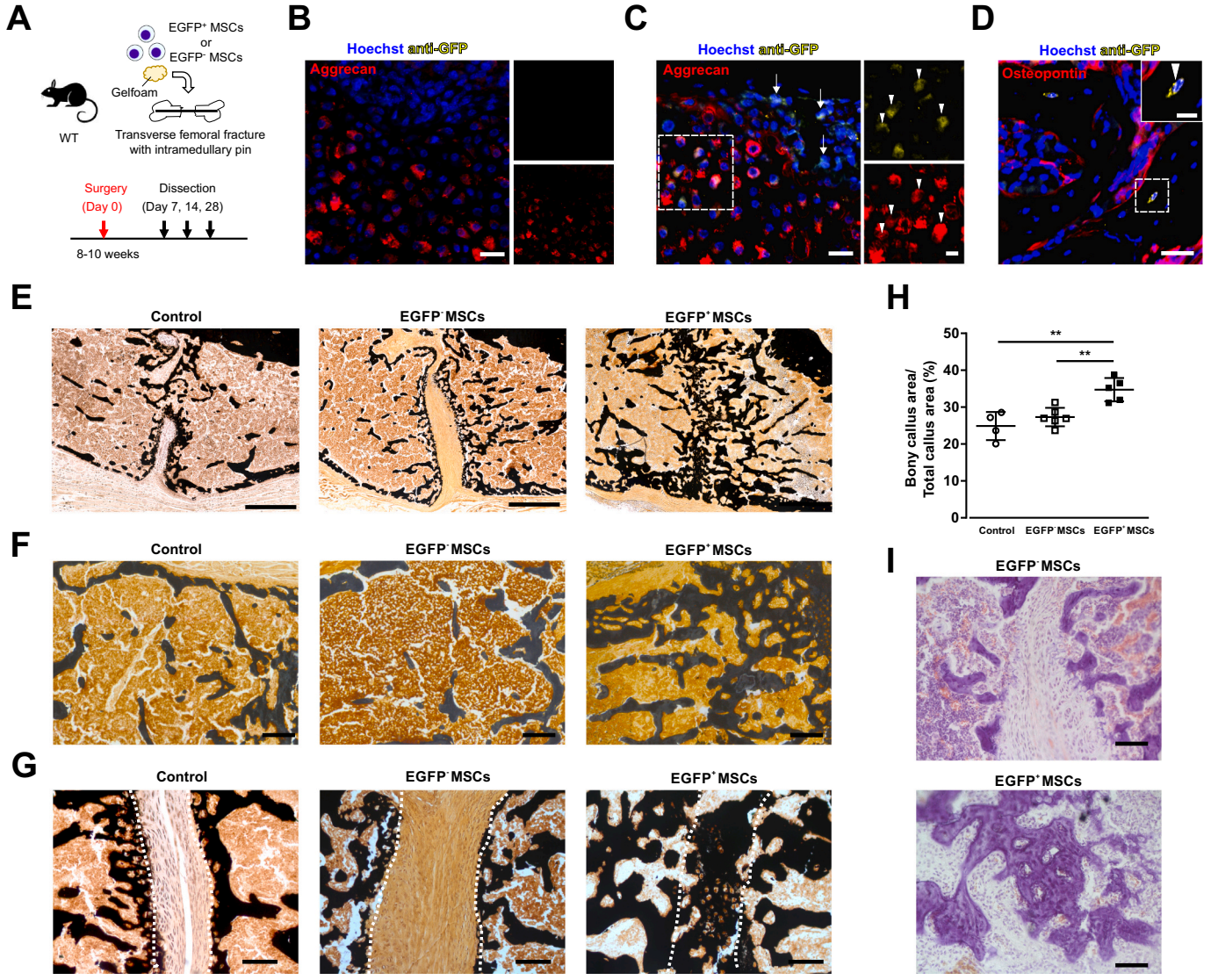

Fig. 5. Grafted CD73-EGFP$^+$ MSCs contribute to the repair of femur lesions.
(A) Experimental scheme and timeline of the transverse femoral fracture model. Cultured EGFP$^+$ and EGFP$^-$ MSCs (5×10^5 cells) were grafted into the fracture site using gelatine sponges. (B, C) Immunofluorescence stainings against EGFP and aggrecan in the regenerative area at day 7 after fracture in saline control (B) and EGFP$^+$ MSC groups (C). There were no EGFP$^+$ cells in the control group (B), but grafted EGFP$^+$ MSCs were observed at the fracture site (C, arrow). Stainings against aggrecan and EGFP proved that grafted EGFP$^+$ MSCs had differentiated into chondrocytes during bone fracture healing (arrowhead); the boxed areas are shown in the magnified images to the right (C). Scale bars 25 μm, magnified image 10 μm. (D) Immunofluorescence staining against EGFP and osteopontin in the regenerative area at day 14 after fracture demonstrated that grafted EGFP$^+$ MSCs contributed to bone trabeculae formation. Scale bar 25 μm, inset 10 μm. (E-G) Representative images of transverse sections stained with von Kossa staining at day 28 after fracture (E). The callus area (F) and fracture site (G) of each treatment group is shown. Broken lines indicate the two ends of the fractured femoral bone (G). Scale bars 100 μm. (H) The areas of the bony callus of each treatment groups were quantified at day 28 after fracture revealing that EGFP$^+$ MSCs did promote fracture repair. (I) Representative images of sections stained with HE showing lamellar bone within the fracture gap in the EGFP$^+$ MSC group. Control group, $n = 4$ mice; EGFP$^-$ MSC group, $n = 6$ mice; EGFP$^+$ MSC group, $n = 5$ mice, one-way ANOVA, **: $p < 0.01$.

into osteoblasts and chondrocytes during fracture repair (Tevlin et al., 2017). We have recently found out using RNAseq analysis that CD200 and CD51 are highly expressed in CD73+ BM-MSC (Breitbach et al., 2018), suggesting that our mouse model could also label these derivatives. In the literature another promising population for bone repair has been reported, namely periosteal stem cells that reside in the periosteum of long bones (Colnot, 2009). These cells are characterized by their robust self-renewal capacity and multipotency. The periosteal stem cells can contribute upon grafting to bone fracture healing by forming cartilage and bone in the callus and are therefore claimed to have higher regenerative capacity than BM-MSCs (Debnath et al., 2018; Duchamp de Lageneste et al., 2018). Interestingly, we have observed that large numbers of periosteal cells are EGFP$^+$, indicating that CD73 expression labels not only BM-MSCs, but also periosteal stem cells. Therefore, future investigations using lineage tracing approaches should provide insight, whether the CD73$^+$ MSCs participating in bone repair originate from specific sites, *i.e.*, periosteal areas, or rather from various sites within the BM.

Besides the apparent beneficial effects of grafting CD73$^+$ MSCs on fracture regeneration *via* forming cartilage and bone callus, MSCs are known to also support healing by paracrine secretion of trophic factors. These influence tissue resident cell proliferation and recruitment (Granero-Molto et al., 2009), but also modulate the inflammatory response. In fact, shifting from a pro-inflammatory to an anti-inflammatory state appears to play a crucial role in stimulating both the initial differentiation of periosteal progenitor cells and transition from cartilage to bone

during endochondral ossification. (Bartholomew et al., 2002; Ortiz et al., 2003). Whether and what role CD73$^+$ MSCs play in the secretion of trophic and immunomodulatory factors affecting bone healing needs to be explored in future studies.

We also obtained information in regard to the neovascularization of the bone fracture site, which is critical for the ongoing repair processes (Maes, 2013). There are at least two types of ECs in the BM, sinusoidal and arteriolar cells, which are critically relevant for the hematopoietic niche (Kunisaki and Frenette, 2014; Itkin et al., 2016). The sECs are specifically marked in our transgenic mouse model, whereas all other types of BM ECs are CD73-EGFP$^-$ during development and at the adult stage (Breitbach et al., 2018). For bone healing, BM ECs are mobilized to the site of the injury, engage in neovascularization and accelerate fracture healing (Maes et al., 2010; Ramasamy et al., 2014). We have observed that robust neovascularization occurred in the internal callus at day 7 after the fracture and that at day 14 remodeling of the newly formed vasculature defined as Vcam1$^+$ ECs took place. We also found that EGFP$^+$ ECs were observed at the internal callus site, indicating that EGFP$^+$ sECs most likely migrated to the regenerative area after the remodeling process of newly formed vessels. This is in line with a recent study demonstrating that CD73$^+$ subpopulations express high levels of cytokines during homeostasis and stress and participate in the early stages of hematopoietic recovery post irradiation (Severe et al., 2019). Thus, our data imply that also BM sECs migrate, contribute to neovascularization of the fracture site and hence could play a critical role in the vessel-mediated healing process.

5. Conclusion

Our study underscores the heterogeneity of BM-MSCs and their differential response and mobilization upon bone fracture. We found that the CD73$^+$ subpopulation of BM- MSCs contributes to the regeneration process of bone fracture healing by promoting callus formation and that also the BM sEC fraction participates in the neovascularization process during bone repair. The precise origin of the CD73$^+$ BM-MSCs and sECs, their spatial distribution, final fate upon completed repair and the involved mechanisms in cell migration and intercellular signaling need to be addressed in future studies. Ideal for this aim would be the generation and use of an inducible CD73-Cre mouse model enabling the tracing of CD73 expressing cells during the fracture repair process.

Supplementary data to this article can be found online at https://doi.org/10.1016/j.bonr.2021.101133.

CRediT authorship contribution statement

Conceptualization, K.K., M.B., and B.K.F.; Investigation, K.K., M.B., M.H., and F.A.S; Resource, B.K.F.; Writing – original Draft, K.K, M.B and B.K.F.; Writing – Review & Editing, K.K., M.B., M.H., F.A.S., and B.K.F.; Visualization, K.K., and M.B.; Project Administration, B.K.F.; Funding Acquisition, B.K.F.

Declaration of competing interest

The authors declare no competing interests.

Acknowledgments

We thank A. Nagy and M. Gertsenstein (Toronto, Canada) for providing the G4 mouse ESC line; E. Endl and the FACS Core facility (Bonn, Germany) for help with flow cytometry; and W. Masson, P. Freitag, and S. Grünberg (Bonn, Germany) for technical assistance. This work was supported by BONFOR O-162.0005 (to M.B.), SENSHIN Medical Research Foundation (to K.K.), The Uehara Memorial Foundation (to K.K.), TERUMO LIFE SCIENCE FOUNDATION (to K. K.), and the Universities of Bonn and of Tsukuba (K.K).

References

Baddoo, M., Hill, K., Wilkinson, R., Gaupp, D., Hughes, C., Kopen, G.C., Phinney, D.G., 2003. Characterization of mesenchymal stem cells isolated from murine bone marrow by negative selection. J.Cell.Biochem. 89 (6), 1235–1249.

Bartholomew, A., Sturgeon, C., Siatskas, M., Ferrer, K., McIntosh, K., Patil, S., Hardy, W., Devine, S., Ucker, D., Deans, R., Moseley, A., Hoffman, R., 2002. Mesenchymal stem cells suppress lymphocyte proliferation in vitro and prolong skin graft survival in vivo. Exp.Hematol. 30 (1), 42–48.

Bradaschia-Correa, V., Josephson, A.M., Egol, A.J., Mizrahi, M.M., Leclerc, K., Huo, J., Cronstein, B.N., Leucht, P., 2017. Ecto-5'-nucleotidase (CD73) regulates bone formation and remodeling during intramembranous bone repair in aging mice. Tissue Cell 49 (5), 545–551.

Breitbach, M., Kimura, K., Luis, T.C., Fuegemann, C.J., Woll, P.S., Hesse, M., Facchini, R., Rieck, S., Jobin, K., Reinhardt, J., Ohneda, O., Wenzel, D., Geisen, C., Kurts, C., Kastenmuller, W., Holzel, M., Jacobsen, S.E.W., Fleischmann, B.K., 2018. In vivo labeling by CD73 marks multipotent stromal cells and highlights endothelial heterogeneity in the bone marrow niche. Cell Stem Cell 22 (2), 262–276 e267.

Carroll, S.H., Wigner, N.A., Kulkarni, N., Johnston-Cox, H., Gerstenfeld, L.C., Ravid, K., 2012. A2B adenosine receptor promotes mesenchymal stem cell differentiation to osteoblasts and bone formation in vivo. J.Biol.Chem. 287 (19), 15718–15727.

Chan, C.K.F., Gulati, G.S., Sinha, R., Tompkins, J.V., Lopez, M., Carter, A.C., Ransom, R. C., Reinisch, A., Wearda, T., Murphy, M., Brewer, R.E., Koepke, L.S., Marecic, O., Manjunath, A., Seo, E.Y., Leavitt, T., Lu, W.J., Nguyen, A., Conley, S.D., Salhotra, A., Ambrosi, T.H., Borrelli, M.R., Siebel, T., Chan, K., Schallmoser, K., Seita, J., Sahoo, D., Goodnough, H., Bishop, J., Gardner, M., Majeti, R., Wan, D.C., Goodman, S., Weissman, I.L., Chang, H.Y., Longaker, M.T., 2018. Identification of the human skeletal stem cell. Cell 175 (1), 43–56 e21.

Chou, D.B., Sworder, B., Bouladoux, N., Roy, C.N., Uchida, A.M., Grigg, M., Robey, P.G., Belkaid, Y., 2012. Stromal-derived IL-6 alters the balance of myeloerythroid progenitors during toxoplasma gondii infection. J.Leukoc.Biol. 92 (1), 123–131.

Colnot, C., 2009. Skeletal cell fate decisions within periosteum and bone marrow during bone regeneration. J. Bone Miner.Res. 24 (2), 274–282.

Costa, M.A., Barbosa, A., Neto, E., Sa-e-Sousa, A., Freitas, R., Neves, J.M., Magalhaes-Cardoso, T., Ferreirinha, F., Correia-de-Sa, P., 2011. On the role of subtype selective adenosine receptor agonists during proliferation and osteogenic differentiation of human primary bone marrow stromal cells. J.Cell.Physiol. 226 (5), 1353–1366.

Crisan, M., Yap, S., Casteilla, L., Chen, C.W., Corselli, M., Park, T.S., Andriolo, G., Sun, B., Zheng, B., Zhang, L., Norotte, C., Teng, P.N., Traas, J., Schugar, R., Deasy, B.M., Badylak, S., Buhring, H.J., Giacobino, J.P., Lazzari, L., Huard, J., Peault, B., 2008. A perivascular origin for mesenchymal stem cells in multiple human organs. Cell Stem Cell 3 (3), 301–313.

D'Alimonte, I., Nargi, E., Lannutti, A., Marchisio, M., Pierdomenico, L., Costanzo, G., Di Iorio, P., Ballerini, P., Giuliani, P., Caciagli, F., Ciccarelli, R., 2013. Adenosine A1 receptor stimulation enhances osteogenic differentiation of human dental pulp-derived mesenchymal stem cells via WNT signaling. Stem Cell Res. 11 (1), 611–624.

Debnath, S., Yallowitz, A.R., McCormick, J., Lalani, S., Zhang, T., Xu, R., Li, N., Liu, Y., Yang, Y.S., Eiseman, M., Shim, J.H., Hameed, M., Healey, J.H., Bostrom, M.P., Landau, D.A., Greenblatt, M.B., 2018. Discovery of a periosteal stem cell mediating intramembranous bone formation. Nature 562 (7725), 133–139.

Dominici, M., Le Blanc, K., Mueller, I., Slaper-Cortenbach, I., Marini, F., Krause, D., Deans, R., Keating, A., Prockop, D., Horwitz, E., 2006. Minimal criteria for defining multipotent mesenchymal stromal cells. The International Society for Cellular Therapy position statement. Cytotherapy 8 (4), 315–317.

Duchamp de Lageneste, O., Julien, A., Abou-Khalil, R., Frangi, G., Carvalho, C., Cagnard, N., Cordier, C., Conway, S.J., Colnot, C., 2018. Periosteum contains skeletal stem cells with high bone regenerative potential controlled by periostin. Nat. Commun. 9 (1), 773.

Erices, A., Conget, P., Minguell, J.J., 2000. Mesenchymal progenitor cells in human umbilical cord blood. Br.J.Haematol. 109 (1), 235–242.

Granero-Molto, F., Weis, J.A., Miga, M.I., Landis, B., Myers, T.J., O'Rear, L., Longobardi, L., Jansen, E.D., Mortlock, D.P., Spagnoli, A., 2009. Regenerative effects of transplanted mesenchymal stem cells in fracture healing. Stem Cells 27 (8), 1887–1898.

Gronthos, S., Mankani, M., Brahim, J., Robey, P.G., Shi, S., 2000. Postnatal human dental pulp stem cells (DPSCs) in vitro and in vivo. Proc.Natl.Acad.Sci.U.S.A. 97 (25), 13625–13630.

Guimaraes-Camboa, N., Cattaneo, P., Sun, Y., Moore-Morris, T., Gu, Y., Dalton, N.D., Rockenstein, E., Masliah, E., Peterson, K.L., Stallcup, W.B., Chen, J., Evans, S.M., 2017. Pericytes of multiple organs do not behave as mesenchymal stem cells in vivo. Cell Stem Cell 20 (3), 345–359 e345.

Itkin, T., Gur-Cohen, S., Spencer, J.A., Schajnovitz, A., Ramasamy, S.K., Kusumbe, A.P., Ledergor, G., Jung, Y., Milo, I., Poulos, M.G., Kalinkovich, A., Ludin, A., Golan, K., Khatib, E., Kumari, A., Kollet, O., Shakhar, G., Butler, J.M., Rafii, S., Adams, R.H., Scadden, D.T., Lin, C.P., Lapidot, T., 2016. Corrigendum: distinct bone marrow blood vessels differentially regulate haematopoiesis. Nature 538 (7624), 274.

Kawamoto, T., 2003 May. Use of a new adhesive film for the preparation of multi-purpose fresh-frozen sections from hard tissues, whole-animals, insects and plants. Arch. Histol. Cytol. 66 (2), 123–143. https://doi.org/10.1679/aohc.66.123.

Kimura, K., Nagano, M., Salazar, G., Yamashita, T., Tsuboi, I., Mishima, H., Matsushita, S., Sato, F., Yamagata, K., Ohneda, O., 2014. The role of CCL5 in the ability of adipose tissue-derived mesenchymal stem cells to support repair of ischemic regions. Stem Cells Dev. 23 (5), 488–501.

Kumar, S., Ponnazhagan, S., 2012. Mobilization of bone marrow mesenchymal stem cells in vivo augments bone healing in a mouse model of segmental bone defect. Bone 50 (4), 1012–1018.

Kunisaki, Y., Frenette, P.S., 2014. Influences of vascular niches on hematopoietic stem cell fate. Int.J.Hematol. 99 (6), 699–705.
Maes, C., 2013. Role and regulation of vascularization processes in endochondral bones. Calcif. Tissue Int. 92 (4), 307–323.
Maes, C., Kobayashi, T., Selig, M.K., Torrekens, S., Roth, S.I., Mackem, S., Carmeliet, G., Kronenberg, H.M., 2010. Osteoblast precursors, but not mature osteoblasts, move into developing and fractured bones along with invading blood vessels. Dev. Cell 19 (2), 329–344.
Matsushita, Y., Nagata, M., Kozloff, K.M., Welch, J.D., Mizuhashi, K., Tokavanich, N., Hallett, S.A., Link, D.C., Nagasawa, T., Ono, W., Ono, N., 2020. A wnt-mediated transformation of the bone marrow stromal cell identity orchestrates skeletal regeneration. Nat.Commun. 11 (1), 332.
Ode, A., Schoon, J., Kurtz, A., Gaetjen, M., Ode, J.E., Geissler, S., Duda, G.N., 2013. CD73/5'-ecto-nucleotidase acts as a regulatory factor in osteo-/chondrogenic differentiation of mechanically stimulated mesenchymal stromal cells. Eur. Cell. Mater. 25, 37–47.
Ortiz, L.A., Gambelli, F., McBride, C., Gaupp, D., Baddoo, M., Kaminski, N., Phinney, D. G., 2003. Mesenchymal stem cell engraftment in lung is enhanced in response to bleomycin exposure and ameliorates its fibrotic effects. Proc.Natl.Acad.Sci.U.S.A. 100 (14), 8407–8411.
Pittenger, M.F., Mackay, A.M., Beck, S.C., Jaiswal, R.K., Douglas, R., Mosca, J.D., Moorman, M.A., Simonetti, D.W., Craig, S., Marshak, D.R., 1999. Multilineage potential of adult human mesenchymal stem cells. Science 284 (5411), 143–147.
Ramasamy, S.K., Kusumbe, A.P., Wang, L., Adams, R.H., 2014. Endothelial notch activity promotes angiogenesis and osteogenesis in bone. Nature 507 (7492), 376–380.
Resta, R., Hooker, S.W., Hansen, K.R., Laurent, A.B., Park, J.L., Blackburn, M.R., Knudsen, T.B., Thompson, L.F., 1993. Murine ecto-5'-nucleotidase (CD73): cDNA cloning and tissue distribution. Gene 133 (2), 171–177.
Sacchetti, B., Funari, A., Michienzi, S., Di Cesare, S., Piersanti, S., Saggio, I., Tagliafico, E., Ferrari, S., Robey, P.G., Riminucci, M., Bianco, P., 2007. Self-renewing osteoprogenitors in bone marrow sinusoids can organize a hematopoietic microenvironment. Cell 131 (2), 324–336.
Severe, N., Karabacak, N.M., Gustafsson, K., Baryawno, N., Courties, G., Kfoury, Y., Kokkaliaris, K.D., Rhee, C., Lee, D., Scadden, E.W., Garcia-Robledo, J.E., Brouse, T., Nahrendorf, M., Toner, M., Scadden, D.T., 2019. Stress-induced changes in bone marrow stromal cell populations revealed through single-cell protein expression mapping. Cell Stem Cell 25 (4), 570–583 e577.
Takedachi, M., Oohara, H., Smith, B.J., Iyama, M., Kobashi, M., Maeda, K., Long, C.L., Humphrey, M.B., Stoecker, B.J., Toyosawa, S., Thompson, L.F., Murakami, S., 2012. CD73-generated adenosine promotes osteoblast differentiation. J.Cell.Physiol. 227 (6), 2622–2631.
Tevlin, R., Seo, E.Y., Marecic, O., McArdle, A., Tong, X., Zimdahl, B., Malkovskiy, A., Sinha, R., Gulati, G., Li, X., Wearda, T., Morganti, R., Lopez, M., Ransom, R.C., Duldulao, C.R., Rodrigues, M., Nguyen, A., Januszyk, M., Maan, Z., Paik, K., Yapa, K. S., Rajadas, J., Wan, D.C., Gurtner, G.C., Snyder, M., Beachy, P.A., Yang, F., Goodman, S.B., Weissman, I.L., Chan, C.K., Longaker, M.T., 2017. Pharmacological rescue of diabetic skeletal stem cell niches. Sci.Transl.Med. 9 (372).
Versaevel, M., Grevesse, T., Gabriele, S., 2012. Spatial coordination between cell and nuclear shape within micropatterned endothelial cells. Nat.Commun. 3, 671.
Zhang, B., 2012. CD73 promotes tumor growth and metastasis. Oncoimmunology 1 (1), 67–70.
Zhou, B.O., Yue, R., Murphy, M.M., Peyer, J.G., Morrison, S.J., 2014. Leptin-receptor-expressing mesenchymal stromal cells represent the main source of bone formed by adult bone marrow. Cell Stem Cell 15 (2), 154–168.
Zuk, P.A., Zhu, M., Mizuno, H., Huang, J., Futrell, J.W., Katz, A.J., Benhaim, P., Lorenz, H.P., Hedrick, M.H., 2001. Multilineage cells from human adipose tissue: implications for cell-based therapies. Tissue Eng. 7 (2), 211–228.